Published November 8, 2010

The F-BAR domain of SRGP-1 facilitates cell–cell adhesion during *C. elegans* morphogenesis

Ronen Zaidel-Bar,[1] Michael J. Joyce,[1] Allison M. Lynch,[2] Kristen Witte,[3] Anjon Audhya,[3] and Jeff Hardin[1,2]

[1]Department of Zoology, [2]Graduate Program in Genetics, and [3]Department of Biomolecular Chemistry, University of Wisconsin–Madison, Madison, WI 53706

Robust cell–cell adhesion is critical for tissue integrity and morphogenesis, yet little is known about the molecular mechanisms controlling cell–cell junction architecture and strength. We discovered that SRGP-1 is a novel component of cell–cell junctions in *Caenorhabditis elegans,* localizing via its F-BAR (Bin1, Amphiphysin, and RVS167) domain and a flanking 200–amino acid sequence. SRGP-1 activity promotes an increase in membrane dynamics at nascent cell–cell contacts and the rapid formation of new junctions; in addition, *srgp-1* loss of function is lethal in embryos with compromised cadherin–catenin complexes. Conversely, excess SRGP-1 activity leads to outward bending and projections of junctions. The C-terminal half of SRGP-1 interacts with the N-terminal F-BAR domain and negatively regulates its activity. Significantly, in vivo structure–function analysis establishes a role for the F-BAR domain in promoting rapid and robust cell adhesion during embryonic closure events, independent of the Rho guanosine triphosphatase–activating protein domain. These studies establish a new role for this conserved protein family in modulating cell–cell adhesion.

Introduction

During development and wound closure, cells that were once separated come into contact and must quickly form robust cell–cell adhesions to ensure tissue integrity. One potentially important factor regulating the formation of new cell–cell adhesions is the contour of cell surfaces as they come into contact. Rapid sealing of epithelial sheets can be catalyzed by filopodia, which physically project into the membrane of adjacent cells, increasing the surface area available for adhesion (Raich et al., 1999; Vasioukhin et al., 2000), yet little is known about the regulation of membrane architecture at cell junctions.

An excellent model for studying this process is epithelial morphogenesis of the nematode *Caenorhabditis elegans* (Piekny and Mains, 2003; Ding et al., 2004; Chisholm and Hardin, 2005). *C. elegans* apical junctions (AJs) contain a conserved cadherin–catenin complex and a DLG-1–AJM-1 complex (Labouesse, 2006; Lynch and Hardin, 2009); the regulation of both is critical during the morphogenetic events of ventral enclosure (Williams-Masson et al., 1997; Costa et al., 1998) and elongation (Priess and Hirsh, 1986; Bossinger et al., 2001; Köppen et al., 2001).

In recent years, BAR (Bin1, Amphiphysin, and RVS167) domain superfamily members have emerged as potent regulators of membrane curvature, involved in endocytosis and filopodium formation (Gallop and McMahon, 2005; Aspenström, 2008; Saarikangas et al., 2009). BAR domains induce positive (inward) curvature (Peter et al., 2004; Weissenhorn, 2005; Gallop et al., 2006; Masuda et al., 2006), whereas I-BAR domains induce negative (outward) curvature (Krugmann et al., 2001; Lee et al., 2007). F-BAR domains of several proteins (FBP17, CIP4, and FCHo2) induce positive curvature similar to BAR domains, but with a flatter angle (Itoh et al., 2005; Tsujita et al., 2006; Henne et al., 2007; Shimada et al., 2007). However, recent work by Guerrier et al. (2009) demonstrated that the F-BAR domain of Slit–Robo GTPase-activating protein (GAP) 2 (srGAP2) functions as an I-BAR domain to induce membrane protrusions, suggesting a more diverse role for F-BAR domains. Here, we show, for the first time, that SRGP-1—the nematode orthologue of mammalian srGAPs—localizes specifically to cell–cell junctions, where it has a role in facilitating rapid and robust cell–cell adhesion during embryonic morphogenesis.

Correspondence to Ronen Zaidel-Bar: biezbr@nus.edu.sg

Abbreviations used in this paper: AJ, apical junction; BAR, Bin1, Amphiphysin, and RVS167; GAP, GTPase-activating protein; PM, plasma membrane; srGAP, Slit–Robo GAP; UTR, untranslated region.

The Rockefeller University Press $30.00
J. Cell Biol.
www.jcb.org/cgi/doi/10.1083/jcb.201005082

Published November 8, 2010

Results and discussion

Basic local alignment search tool analysis identified *srgp-1* as the single *C. elegans* orthologue of mammalian srGAP proteins. Discovered as downstream effectors of the Slit–Robo neuronal guidance pathway (Wong et al., 2001), srGAPs were subsequently found in vitro to act as negative regulators of neuronal cell migration (Endris et al., 2002; Soderling et al., 2002; Yang et al., 2006; Vogt et al., 2007; Guerrier et al., 2009). Nematode SRGP-1 shares 33% identity and 53% similarity with human srGAP1 within its first 724 aa, including the F-BAR and RhoGAP domains (Fig. S1). There is little conservation between nematode and human sequences along the last third of the protein, which includes an SH3 domain in mammalian srGAPs that is not conserved in SRGP-1.

To determine the expression pattern of *srgp-1*, we examined a transcriptional reporter in which cytoplasmic GFP is driven by the *srgp-1* promoter (Dupuy et al., 2007). We detected transcription as early as 100 min into development in all cells except the germline (Fig. S2 A). Later in embryogenesis, expression was restricted to neurons, epidermal cells, and cells of the pharynx. In adults, expression was found in head and tail neurons and in neurons along the body, in addition to strong expression in the pharynx and spermatheca (Fig. S2 B).

To address the subcellular localization of SRGP-1, we constructed a translational fusion containing *srgp-1* cDNA C terminally fused with GFP driven by the *srgp-1* promoter. In embryos, SRGP-1::GFP localized specifically to sites of contact between cells. When first detected, ∼150 min after first cleavage, SRGP-1::GFP appeared along most cell–cell contacts (Fig. 1 A). After epidermal differentiation, SRGP-1 appeared uniformly along all AJs, where it colocalized with cadherin complex components (Fig. 1, A and B). SRGP-1 did not colocalize appreciably with DLG-1/discs large and AJM-1, but appeared to reside predominantly apical to the DLG-1–AJM-1 complex (Fig. 1 C). Immunostaining of endogenous SRGP-1 with a polyclonal antibody validated the observations made with the GFP-tagged protein (Fig. 1 D).

To test whether SRGP-1 localization at AJs depends on HMR-1/cadherin, we knocked down *hmr-1* transcripts by injection RNAi. The absence of HMR-1 protein in the hypodermis was evident by the lethal "hammerhead" phenotype (Costa et al., 1998) and confirmed by immunostaining (unpublished data). Significantly, in the absence of HMR-1, SRGP-1 maintained its pattern of localization at junctions (Fig. 2 A). This result indicates that SRGP-1 localizes to junctions in a cadherin-independent manner. srGAPs were first identified in mammalian cells as downstream effectors of the Robo receptor (Wong et al., 2001). This interaction is mediated by the SH3 domain of srGAPs (Li et al., 2006), which SRGP-1 lacks (Fig. S1). Nonetheless, we tested whether the worm homologue of Robo, SAX-3, is responsible for recruiting SRGP-1 to the junction by injecting the *srgp-1::gfp* transgene into a *sax-3*–null strain, *sax-3(ky123)*. Importantly, the localization of SRGP-1 in the *sax-3*–null background was identical to wild-type embryos (Fig. 2 B).

To identify the region in SRGP-1 responsible for localization to cell–cell junctions, we engineered a series of deletions in the

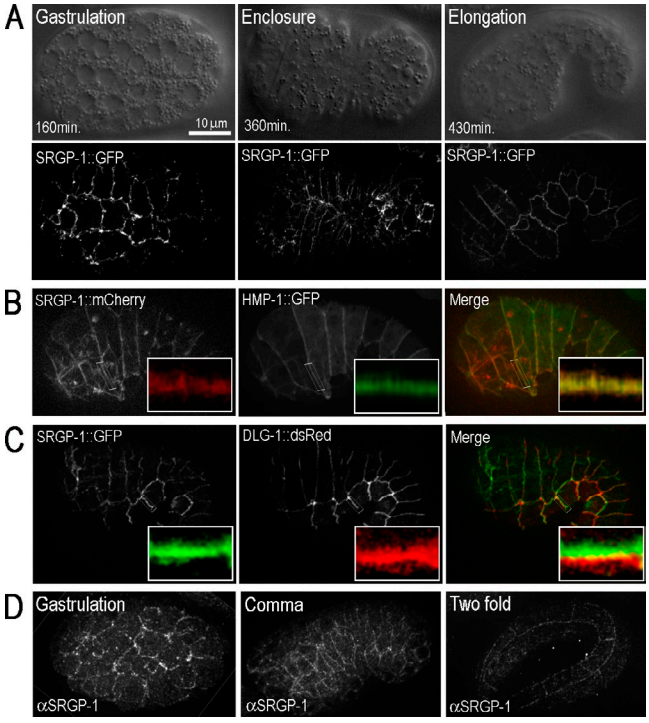

Figure 1. **SRGP-1 localizes to cell–cell junctions in *C. elegans* embryos.** (A) Nomarski and confocal projections of SRGP-1::GFP demonstrate localization at cell–cell contacts throughout embryogenesis. (B) SRGP-1::mCherry and HMP-1::GFP in an elongating embryo show colocalization of the two proteins at epidermal adherens junctions. (C) SRGP-1::GFP and DLG-1::dsRed in an elongating embryo show partial colocalization, where SRGP-1 occupies a space mostly apical to DLG-1. Insets are the side views of the boxed junctions. (D) Immunolabeling of endogenous SRGP-1 with an antibody validates SRGP-1::GFP localization.

srgp-1::gfp transgene. The various constructs were expressed at similar levels, as determined by quantification of fluorescence intensity (unpublished data). We examined their localization pattern at three developmental stages: early gastrulation (∼100 cells), epidermal enclosure, and elongation (Fig. 2, C–G). Deletion of the F-BAR domain led to the loss of junctional localization and accumulation in the cytoplasm in the early embryo. Interestingly, during enclosure, some junctional localization could be detected, which increased during elongation. However, it was not as uniform as the full-length protein, and cytoplasmic localization persisted (Fig. 2 C). Expression of the F-BAR domain alone resulted in robust targeting to the plasma membrane (PM), but significantly, the distribution was uniform throughout the PM surface (Fig. 2 D). Full junctional targeting was achieved by adding 200 aa immediately C terminal to the F-BAR domain (Fig. 2 E). Consistent with this result, deletion of the GAP domain or of the C terminus resulted in a wild type–like distribution of the fusion protein (Fig. 2, F and G). These results suggest that SRGP-1 is localized to cell–cell junctions by two complementary mechanisms: (1) targeting to the PM by its F-BAR domain and (2) an interaction with a putative junctional targeting domain located within the 200 aa between the F-BAR and RhoGAP domains. Interestingly, cortical localization in the early embryo was dependent on the F-BAR domain, but not so in the epidermis, suggesting alternative mechanisms for its localization in different cell types.

Published November 8, 2010

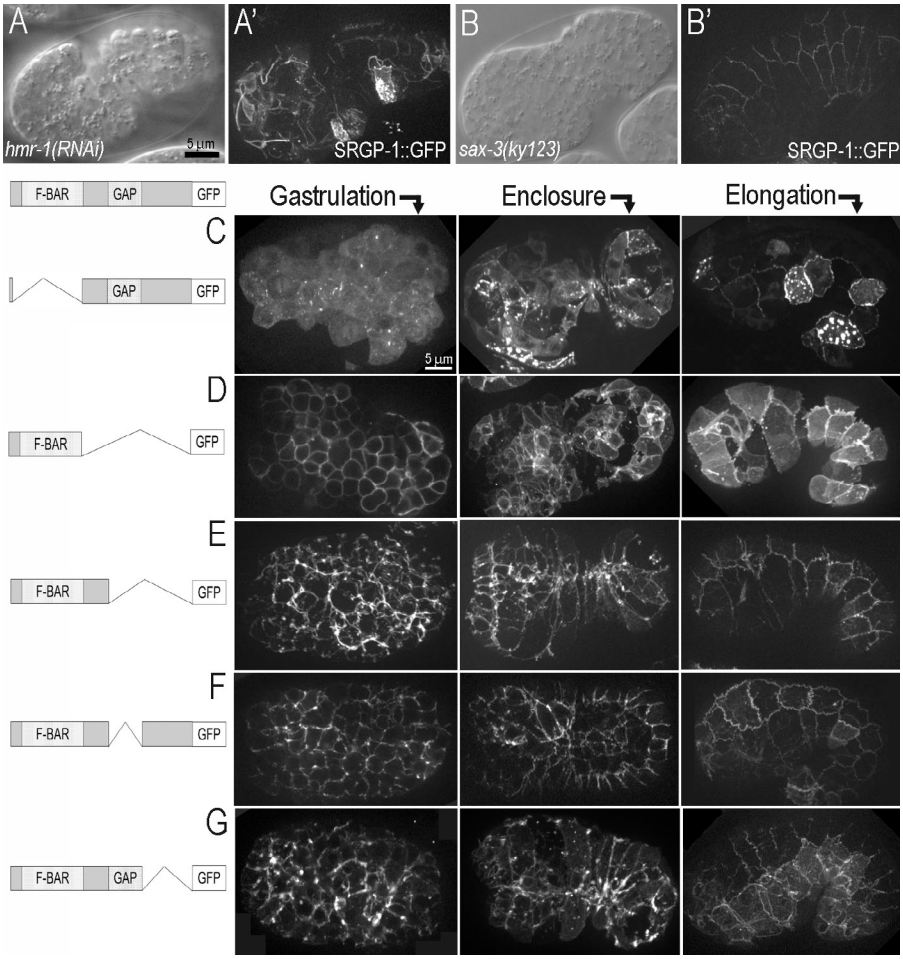

Figure 2. **Determinants of SRGP-1 localization.** (A) SRGP-1::GFP retains its junctional localization upon *hmr-1*/cadherin depletion via RNAi. (B) SRGP-1::GFP localizes to junctions in embryos homozygous for a null allele of *sax-3*/Robo, *ky123*. (C) Deletion of the F-BAR domain abolishes SRGP-1 junctional localization in the early embryo, but later, SRGP-1(ΔF-BAR) is recruited to epidermal AJs during elongation. (D) The F-BAR domain alone distributes uniformly over the entire PM. (E) A 200-aa sequence beyond the F-BAR domain is sufficient to confer junctional localization at all developmental stages. (F) The GAP domain is dispensable for SRGP-1 localization. (G) Deletion of the C terminus of SRGP-1 results in largely wild-type distribution, with some aggregates.

To address the role of SRGP-1 at cell junctions, we knocked it down using RNAi. Western blot analysis indicated depletion of endogenous SRGP-1 to levels below detection (Fig. S3 A). Surprisingly, knockdown of *srgp-1* had no overt effect on embryogenesis. Similarly, worms homozygous for the mutant allele *srgp-1(ok300)* appeared wild type. We tested for redundancy with another F-BAR and RhoGAP protein named TAG-341 by knocking down *tag-341* by RNAi in *srgp-1(ok300)* worms; we also performed double *tag-341(RNAi);srgp-1(RNAi)* knockdowns. Neither of these tests resulted in any overt abnormalities (unpublished data). We conclude that SRGP-1 plays a modulatory role at cell–cell junctions.

To identify sublethal effects of *srgp-1* loss of function, we used confocal microscopy to follow HMP-1::GFP dynamics during ventral enclosure. Careful measurements of the rate of migration revealed no difference between control and *srgp-1 (RNAi)* cells (Fig. S3 B). However, we observed a dramatic reduction in the amount of membrane ruffling at the leading edge of enclosing epidermal cells in *srgp-1(RNAi)* embryos (Video 1). Importantly, we found that once epidermal cells reached the ventral midline, they formed junctions significantly more slowly in *srgp-1(RNAi)* compared with control embryos (Fig. 3 A). In wild-type embryos, it took opposing cells spaced 1 µm apart 6.0 ± 1 min ($n = 5$) to form a clear junction, whereas in *srgp-1(RNAi)* embryos, the same process took 10.8 ± 3 min ($n = 6$; Student's t test, $P < 0.005$), suggesting that *srgp-1* activity promotes rapid adhesion during the initiation of new cell–cell contacts.

AJ components that are not essential on their own for epidermal morphogenesis often reveal their supportive roles in a sensitized background (Pettitt et al., 2003; Sheffield et al., 2007; Lockwood et al., 2008). We tested whether this is the case for *srgp-1* using the *hmp-1* allele, *fe4* (Pettitt et al., 2003), and an *hmp-2* hypomorph, *qm39* (Hekimi et al., 1995). Upon knockdown of *srgp-1* by RNAi, the embryonic lethality of *hmp-1(fe4)* rose from 60% ($n = 466$) to 100% ($n = 404$), and that of *hmp-2(qm39)* climbed from 5% ($n = 710$) to 76% ($n = 356$). In addition to the increase in lethality, *srgp-1* knockdown led to earlier and more severe defects during embryogenesis, as revealed by Nomarski 4D videos and confocal microscopy (Fig. 3, B and C; and Video 2). No *hmp-2(qm39)* embryos had enclosure defects, whereas ∼25% of *hmp-2(qm39);srgp-1(RNAi)* embryos failed to seal the gastrulation cleft (Fig. S3 C) or the epidermis (Fig. 3 C). These results are consistent with our analysis of ventral midline sealing and further suggest that SRGP-1 aids the formation of rapid and robust adhesions at the ventral midline.

To verify the results obtained by RNAi knockdown, we examined *hmp-2(qm39);srgp-1(ok300)* mutants. *qm39/qm39;ok300/+* worms were viable, and their progeny did not show increased lethality relative to *qm39* homozygotes. However, progeny of double homozygotes exhibited 98% embryonic lethality, and the 2% that hatched arrested as L1 larvae.

Published November 8, 2010

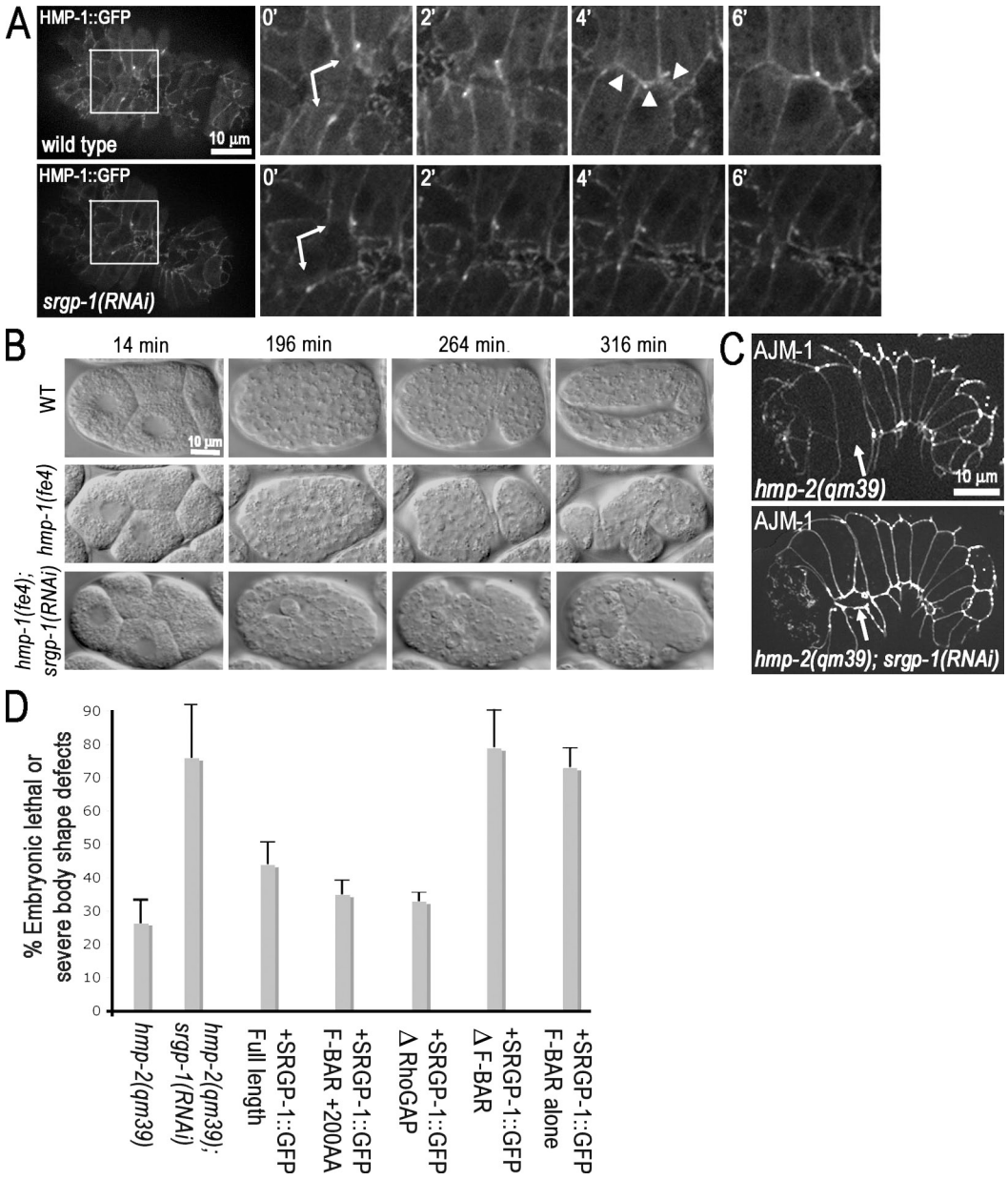

Figure 3. **Loss of *srgp-1* function slows junction formation and enhances the embryonic lethality of α- or β-catenin hypomorphs.** (A) Ventral enclosure visualized by HMP-1::GFP. In the first frame, the leading cells are ∼1 µm apart (arrows). Junctions form faster (arrowheads) in control versus *srgp-1(RNAi)* embryos. The boxes in the images on the left outline the areas that are shown in the time series from 0 to 6 min. (B) Time-lapse Nomarski of a developing wild-type embryo alongside an *hmp-1(fe4)* mutant, which develops lumps during elongation, and an *hmp-1(fe4);srgp-1(RNAi)* embryo, which fails to close the gastrulation cleft and then ruptures. WT, wild type. (C) Comparison of cell junctions using AJM-1::GFP in *hmp-2(qm39)* and *hmp-2(qm39);srgp-1(RNAi)* embryos demonstrates a gap between epidermal cells at the midline in the double mutant (arrows). (D) Rescue of embryonic lethality associated with the knockdown of endogenous *srgp-1* in *hmp-2(qm39)* mutants by the expression of transgenic full-length *srgp-1* or deletion constructs that contain the F-BAR and junctional targeting sequence. Error bars denote SEM ($n > 250$).

To test whether SRGP-1 plays a role in earlier closure events, we examined the process of gastrulation cleft closure (Nance and Priess, 2002). We used a cytoplasmic GFP expressed in neuroblasts (*Pkal-1*::*gfp*) to visualize cleft closure in wild-type, *hmp-2(qm39)*, and *hmp-2(qm39);srgp-1(RNAi)* embryos. Once cells came into contact in wild-type embryos, they rapidly adhered and were never observed to separate again (Video 3). In contrast, in *hmp-2(qm39)* embryos, cells at the cleft sometimes adhered and then separated again. In *hmp-2 (qm39);srgp-1(RNAi)* embryos, the weak adhesion phenotype was exacerbated: after initial movement ventrally, opposing cells were frequently observed to move apart (Fig. S3, D and E; and Video 3). In conclusion, SRGP-1 activity appears to facilitate the adhesion of neuroblasts as well as epidermal cells.

To determine whether the F-BAR and/or the RhoGAP domains of SRGP-1 are important for its function as a positive regulator of cell–cell adhesion, we took advantage of the fact that our *srgp-1::gfp* transgenes contain the 3′ untranslated region (UTR) of *unc-54*. We expressed full-length *srgp-1::gfp* and each of the deletion transgenes in *hmp-2(qm39)* worms and then

Published November 8, 2010

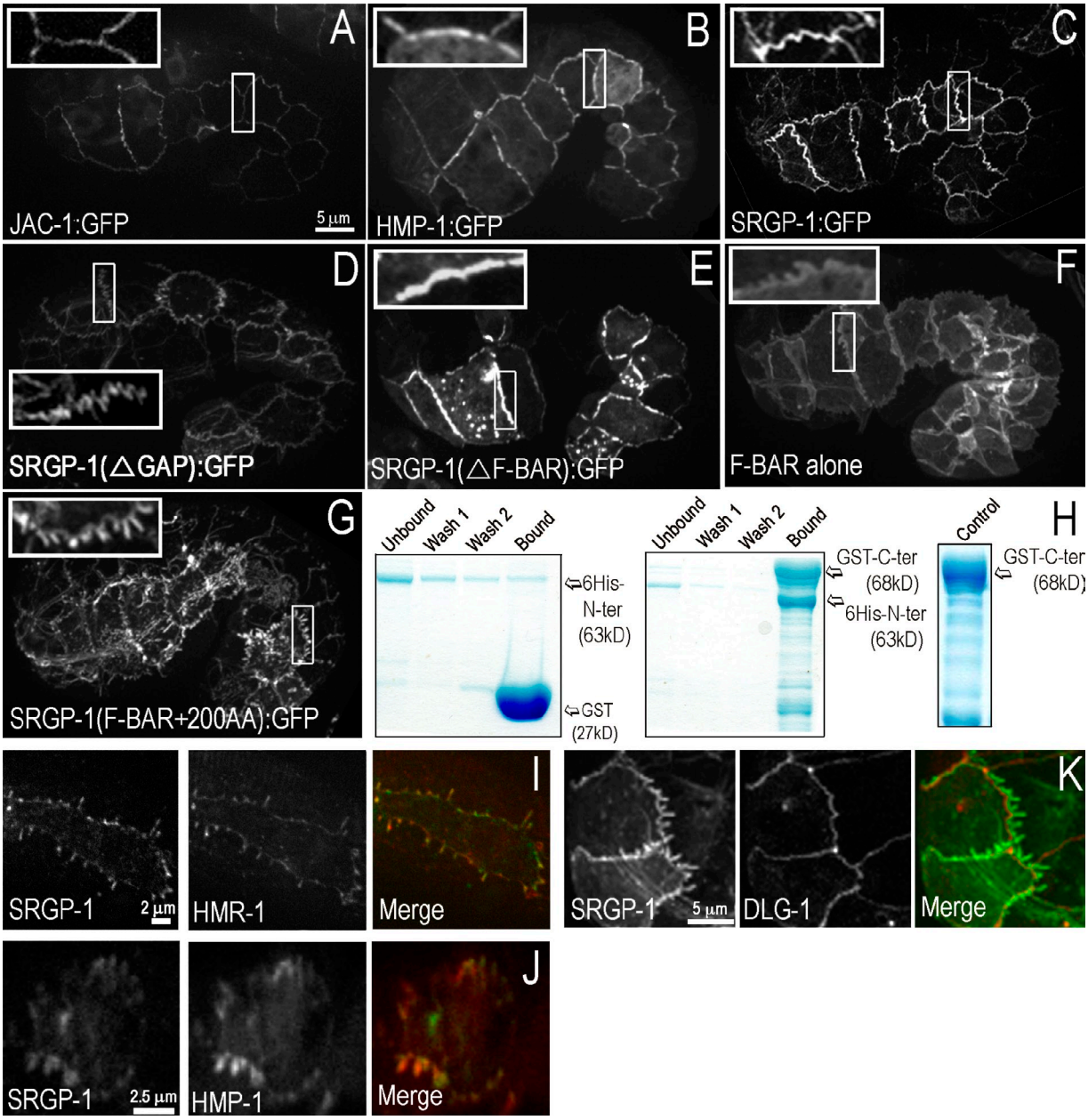

Figure 4. **Overexpression of SRGP-1::GFP induces F-BAR–dependent bending at cell–cell junctions.** (A and B) Overexpressed JAC-1/p120-catenin (A) and HMP-1 (B) appear as straight lines at AJs. (C) Overexpressed SRGP-1 has a wavy appearance. (D–G) The wavy appearance remains upon RhoGAP domain deletion (D) but is abolished when the F-BAR domain is deleted (E). The F-BAR domain alone has a mild effect on membranes (F). However, coupled with the junctional targeting sequence, it becomes very potent in deforming junctions (G). Insets show magnification of the indicated areas. (H) The N-terminal half of SRGP-1 (containing the F-BAR domain and junctional targeting domain) tagged with 6× His does not bind significantly to GST alone (left), but it does binds strongly to the C-terminal half of SRGP-1 tagged with GST (middle), which on its own does not degrade to give a similar band (right). (I–K) Immunostaining of SRGP-1::GFP embryos with an αHMR-1 antibody (I) and embryos coexpressing SRGP-1::mCherry and HMP-1::GFP (J) show a high degree of colocalization between cadherin–catenin complex components and SRGP-1. In contrast, DLG-1::dsRed is not perturbed by SRGP-1::GFP expression and does not colocalize in induced projections (K).

knocked down endogenous *srgp-1* mRNA by targeting its 3′ UTR, without affecting the expression of the transgene, allowing us to score for rescue of synergistic lethality.

Targeting the 3′ UTR of endogenous *srgp-1* in *hmp-1(qm39)* worms led to 31% embryonic lethality, 46% of larvae with severe body shape defects, and 23% superficially wild-type larvae (Fig. 3 D). Expression of full-length SRGP-1::GFP was able to substantially compensate for loss of endogenous SRGP-1: embryonic lethality declined to 15%, and 57% of larvae appeared wild type. Importantly, SRGP-1::GFP(F-BAR + 200 aa) rescued similarly to full length. Comparable rescue was also obtained with SRGP-1::GFP(ΔGAP). In contrast, transgenes missing the F-BAR domain or encoding only the F-BAR domain were not able to rescue (Fig. 3 D). Thus, the F-BAR domain and the junctional targeting domain of *srgp-1* are essential for its adhesion-promoting activity at junctions, whereas the RhoGAP domain is not necessary.

In light of the importance of the F-BAR domain for SRGP-1 activity, we investigated the topology of cell–cell junctions in

Published November 8, 2010

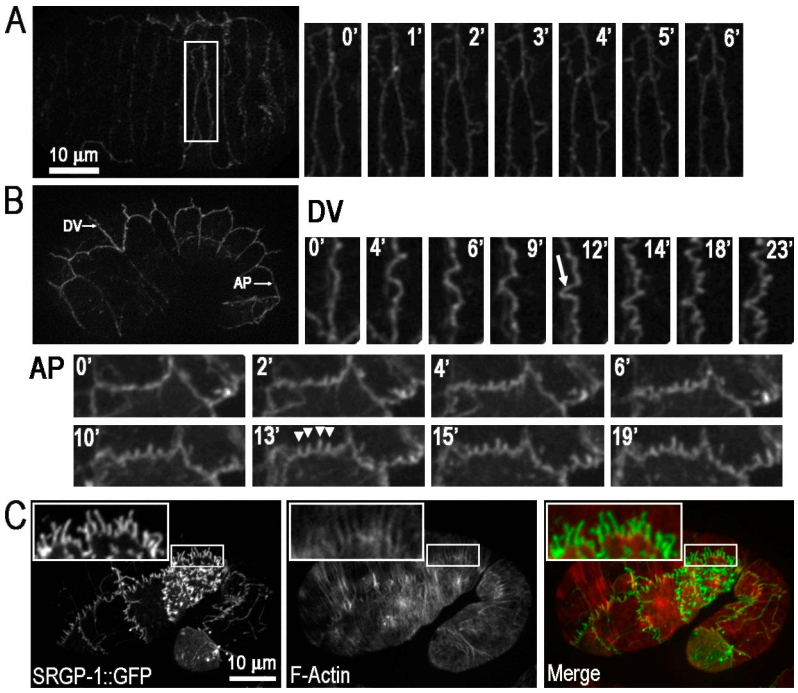

Figure 5. **Dynamics of SRGP-1–induced bending of junctions.** (A) SRGP-1::GFP in dorsal epidermal cells shows dynamic bending along the junction. The box in the image on the left outlines the area that is shown in the time series from 0 to 6 min on the right. (B) SRGP-1::GFP dynamics along dorsal–ventral (DV) and anterior–posterior (AP) junctions in an elongating embryo show more permanent bending of the dorsal–ventral junction (arrow) and the appearance of projections along the anterior–posterior junction (arrowheads). (C) SRGP-1::GFP–induced projections do not appear to colocalize with F-actin as seen in a Z stack projection of an embryo expressing VAB-10(actin-binding domain)::GFP. Insets show magnification of the indicated areas.

embryos expressing SRGP-1::GFP constructs and compared them with embryos expressing the junctional markers HMP-1::GFP or JAC-1::GFP. The cell–cell junctions delineated by HMP-1::GFP and JAC-1::GFP were invariably straight, regardless of expression level or embryonic stage (Fig. 4, A and B). In embryos expressing moderate levels of SRGP-1::GFP, junctions were also straight (Fig. 1 A). In contrast, cell–cell junctions of cells expressing high levels of SRGP-1::GFP displayed a high degree of bending (Fig. 4 C). This effect on junction topology was independent of the RhoGAP domain (Fig. 4 D) and dependent on the F-BAR domain because its deletion resulted in straight junctions (Fig. 4 E). Expression of the F-BAR domain alone resulted in some membrane bending; however, it was not concentrated at junctions (Fig. 4 F). Strikingly, expression of the F-BAR domain along with the junction-targeting sequence resulted in dramatic remodeling of the cell–cell junction interface (Fig. 4 G).

The observation that deletion of the C-terminal half of SRGP-1 resulted in more pronounced membrane-bending activity compared with the full-length protein suggested that the C terminus may perform an inhibitory role. To test whether the C-terminal half of SRGP-1 can interact directly with the N-terminal half, we performed an in vitro binding assay with bacterially expressed recombinant proteins. We found that the His-tagged N-terminal half of SRGP-1 directly binds to the GST-tagged C-terminal half of SRGP-1 (Fig. 4 H). Collectively, these results suggest SRGP-1 may be regulated by a conformational switch. Similar regulation by autoinhibition was recently reported for the F-BAR protein syndapin1, in which an N-terminal F-BAR domain is inhibited by a C-terminal SH3 domain (Rao et al., 2010).

To determine whether the abnormal topology induced by SRGP-1::GFP affects the whole cell–cell junction, we examined embryos coexpressing full-length SRGP-1::mCherry with either HMP-1::GFP or DLG-1::GFP, and we immunostained embryos expressing full-length SRGP-1::GFP for HMR-1. Importantly, we found nearly complete colocalization of the cadherin–catenin complex components with SRGP-1 along membrane bends and projections (Fig. 4, I and J), whereas DLG-1 remained behind (Fig. 4 K).

Finally, we followed the dynamics of junctional SRGP-1::GFP at different developmental stages using time-lapse microscopy. In preelongation embryos, we observed temporary bends at junctions that straightened out within minutes (Fig. 5 A and Video 4). During elongation, we observed bends, folds, and projections in epidermal AJs that persisted for many minutes (Fig. 5 B and Video 4). Bends were more prevalent in shortening junctions along the dorsal–ventral axis, and projections were more prevalent in elongating junctions along the anterior–posterior axis. The majority of these projections either remained stable or grew longer (up to ∼1.5 µm), whereas only a small fraction retracted. Importantly, based on embryos mosaically expressing SRGP-1::GFP, we conclude that the bending and projections were in an outward direction.

Our finding that the F-BAR domain of SRGP-1 induces negative membrane bending is consistent with a recent study by Guerrier et al. (2009), who reported filopodia-like protrusions induced by the F-BAR domain of mammalian srGAP2. Recently, Shimada et al. (2010) postulated that another F-BAR domain protein, Pacsin2, facilitates protrusions by inducing positive curvature at the neck of the protrusion. It is unlikely that this is the case with SRGP-1 because it is localized all along the projections and is not restricted to their base. It remains to be seen whether the F-BAR domains of srGAPs self-assemble into helical coats, as has been shown in vitro for the F-BAR domains of CIP4 and FBP17 (Frost et al., 2008), and whether SRGP-1 cooperates with other actin regulators, such as neural Wiskott-Aldrich syndrome protein, as has been shown for syndapin (Dharmalingam et al., 2009).

Published November 8, 2010

It is possible the F-BAR domain of SRGP-1 functions like an I-BAR domain, whereby initial deformation of the membrane is followed by actin polymerization into the generated space (Lim et al., 2008; Yang et al., 2009). However, using an F-actin reporter and phalloidin staining to test for the presence of actin in the SRGP-1::GFP–induced projections, we could not detect any F-actin along their length (Fig. 5 C and not depicted), suggesting they are formed and stabilized independently of actin polymerization.

The phenotypes we observe in SRGP-1–overexpressing embryos suggest the normal activity of SRGP-1 at junctions is to induce a level of curvature that is optimized for robust adhesion. However, we cannot rule out other effects SRGP-1 might have on the junction, such as modulating the rigidity of the membrane. SRGP-1's membrane-modulating activity becomes essential under conditions in which the cadherin–catenin complex function is compromised, such as in *hmp-1* or *hmp-2* hypomorphic mutants. How membrane curvature at junctions affects cell–cell adhesion is not entirely clear, but one straightforward possibility is that it increases the surface area between contacting cells, thereby increasing the available membrane surface area for adhesive contact formation. The loss of membrane ruffling we observed during ventral midline sealing in *srgp-1(RNAi)* embryos is consistent with this possibility. In conclusion, our results establish SRGP-1 as a potent regulator of cell–cell junction architecture, with important ramifications for cell adhesion and morphogenesis.

Materials and methods

Strains and alleles

C. elegans strains were grown at 20°C. The wild type used was N2 Bristol. Transgenic lines carrying jcEx arrays were obtained via DNA injections into the gonads of hemaphrodites using a micromanipulation device (Narishige International USA, Inc.). The constructs were injected at 2 ng/µl, along with 20 ng/µl F35D3 DNA and 30 ng/µl *rol-6(su1006)* or $P_{ttx\text{-}3}$*::dsRed* DNA as a coinjection marker. Some nematode strains used in this work were provided by the Caenorhabditis Genetics Center, which is funded by the National Institutes of Health National Center for Research Resources. F-actin reporter strains were a gift from M. Labouesse (Institute of Genetics and Molecular and Cellular Biology, Strasbourg, France). The following alleles were used in this study: LGI, *hmp-2(qm39)*; LGIV, *srgp-1(ok300)*; LGV, *hmp-1(fe4)*; and LGX, *sax-3(ky123)*. The *hmp-1(fe4)* allele is a missense mutation (S823F) in the actin-binding domain of HMP-1. The *hmp-2(qm39)* allele is a missense mutation (T358I) in the eighth armadillo repeat (Costa, M., personal communication). Other alleles are described in WormBase.

The following integrated arrays were used: *otIs33[Pkal-1::GFP]*, *jcIs17[hmp-1::gfp* and *dlg-1::dsRed]*, *jcIs1[ajm-1::gfp* and *rol-6(su1006)]*, *jcIs24[jac-1::gfp* and *rol-6(su1006)]*, and *mcIs40[*$P_{lin\text{-}26}$*::vab-10(actin-binding domain)::mCherry* and *myo-2::gfp]*. The following extrachromosomal arrays were used: sEx10607[rCesF12F6.5::GFP + pCeh361], *jcEx135[*$P_{srgp\text{-}1}$*::srgp-1(cDNA, full length)::gfp, rol-6(su1006)]*, *jcEx136[*$P_{srgp\text{-}1}$*::srgp-1(cDNA, AA344-1059), rol-6(su1006)]*, *jcEx137[*$P_{srgp\text{-}1}$*::srgp-1(cDNA, ΔAA540-685), rol-6(su1006)]*, *jcEx138[*$P_{srgp\text{-}1}$*::srgp-1(cDNA, ΔAA562-564), rol-6(su1006)]*, *jcEx139[*$P_{srgp\text{-}1}$*::srgp-1(cDNA, AA1-684), rol-6(su1006)]*, *jcEx140[*$P_{srgp\text{-}1}$*::srgp-1(cDNA, AA1-343), rol-6(su1006)]*, *jcEx145[*$P_{srgp\text{-}1}$*::srgp-1(cDNA, AA1-539), rol-6(su1006)]*, *jcEx147[*$P_{srgp\text{-}1}$*::srgp-1(cDNA, full length)::mCherry, Pttx-3::dsRed]*, *jcEx72[hmp-1::GFP, rol-6(su1006)]*, and *mcEx227[*$P_{lin\text{-}26}$*::Vab-10(actin-binding domain)::gfp, rol-6(su1006)]*.

Molecular biology and biochemistry

The *srgp-1* promoter (3 kb upstream of the start codon amplified from fosmid WRM0621aC06) was inserted into PstI and BamHI sites of the Fire laboratory vector pPD95.75. The ORF of *srgp-1* was amplified from a pDONR201 vector (Thermo Fisher Scientific) and inserted between an NheI site (introduced by the reverse primer of the promoter) and SmaI. All deletion constructs were made by circle PCR using the high fidelity polymerase *Pfu* (Agilent Technologies) and the full-length plasmid as a template.

DNA encoding the last 540 aa of SRGP-1 was cloned into pGEX4T-1 (GE Healthcare) using SalI and NotI and expressed in BL21-Gold (Agilent Technologies) in parallel with the empty vector encoding GST alone. DNA encoding the first 520 aa of SRGP-1 was cloned into pET15b (EMD) with a His tag using NdeI and BamHI. After lysis and sonication, both GST and GST::SRGP-1–C terminus were bound to glutathione resin, loaded onto a column, and thoroughly washed. His-tagged SRGP-1–N terminus was similarly purified with Ni-NTA agarose (Sigma-Aldrich), and after elution, the buffer was replaced by dilution and centrifuge concentration with GST wash buffer. Protein concentrations were determined by Coomassie staining, and then equal amounts of the two SRGP-1 fragments were incubated for 2.5 h at 4°C with agitation. After washing with three resin volumes, samples were boiled in sample buffer, run on a gel, and Coomassie stained, and the gels were photographed using a charge-coupled device camera (Scion) attached to a computer (Mac Mini; Apple) running ImageJ software (National Institutes of Health).

RNAi

Knockdown of gene expression by RNAi was performed as previously described (Timmons, 2006). Knockdown of *srgp-1* was performed by feeding RNAi using sequenced clones from the Ahringer laboratory library, whereas knockdown of *hmr-1* was performed by injection of 2 µg/µl RNA transcribed in vitro from a Kohara clone using MegaScript T3 and T7 kits (Applied Biosystems). For knockdown of endogenous *srgp-1* mRNA, its 3′ UTR was targeted using a genomic region 295 bp long starting 47 bp after the stop codon, which was cloned into L4440 and transformed into HT115(DE3) bacteria.

Immunostaining of embryos

Embryos were harvested by bleaching gravid hemaphrodites and placed on poly-L-lysine–coated ring slides under a coverslip. Next, embryos were freeze cracked and fixed for 15 min in methanol at −20°C. After a 30-min wash in PBS with Tween and blocking with 1% BSA in PBS with Tween, samples were incubated with primary antibodies overnight at 4°C. Secondary antibodies were incubated for 1 h at room temperature. Slides were mounted in antifade reagent (Slowfade Gold; Invitrogen) and sealed with nail polish. Primary antibodies used were rabbit anti–SRGP-1, raised against the last 300 aa of the protein (ProteinTech Group); rabbit anti–HMR-1, raised against the intracellular C terminus (Covance); and goat anti–HMP-2 (Santa Cruz Biotechnology, Inc.). Secondary antibodies were obtained from Jackson ImmunoResearch Laboratories, Inc.

Microscopy and image analysis

For time-lapse videos, embryos were excised from hemaphrodites and then mounted and sealed in M9 on 2% agarose pads. Nomarski 4D microscopy was performed on a camera (Optiphot-2; Nikon) using a PlanApo 60× 1.4 NA lens. Image acquisition was controlled by ImageJ using custom macros/plug-ins. Fluorescently tagged proteins were imaged on a spinning-disk confocal setup (PerkinElmer) based on a microscope (Eclipse E600; Nikon), scanhead (CSU10; Yokogawa), and charge-coupled device camera (ORCA-ER; Hamamatsu). All videos were acquired using a PlanApo total internal reflection fluorescence 100× 1.45 NA lens (Nikon) using Ultraview software (PerkinElmer) at 20°C.

Images were analyzed using ImageJ and Volocity (PerkinElmer), and figures were prepared with Photoshop (Adobe). Mean and standard errors of the mean were calculated in Excel (Microsoft).

Online supplemental material

Fig. S1 shows a sequence alignment of SRGP-1 with mammalian srGAPs. Fig. S2 shows the expression pattern of the *srgp-1* promoter. Fig. S3 shows phenotypes of *srgp-1* knockdown in catenin hypomorphs, including gastrulation cleft closure defects. Video 1 shows ventral enclosure in wild-type and *srgp-1(RNAi)* embryos. Video 2 shows morphogenetic failure in *hmp-1(fe4);srgp-1(RNAi)* double mutants. Video 3 shows gastrulation cleft closure in wild type and mutants. Video 4 shows the dynamics of SRGP-1::GFP at various developmental stages. Online supplemental material is available at http://www.jcb.org/cgi/content/full/jcb.201005082/DC1.

We thank Lukas Neukomm (University of Zürich, Switzerland) for sharing unpublished data, Jaeda Coutinho-Budd for comments on the manuscript, and the Caenorhabditis Genetics Center for strains.

R. Zaidel-Bar was supported by National Institutes of Health postdoctoral training grant GM078747, and a Machiah Foundation fellowship. Research was funded by National Institutes of Health grants GM058038 awarded to J. Hardin and GM088151 awarded to A. Audhya.

Submitted: 17 May 2010
Accepted: 11 October 2010

References

Aspenström, P. 2008. Roles of F-BAR/PCH proteins in the regulation of membrane dynamics and actin reorganization. *Int. Rev. Cell Mol. Biol.* 272:1–31. doi:10.1016/S1937-6448(08)01601-8

Bossinger, O., A. Klebes, C. Segbert, C. Theres, and E. Knust. 2001. Zonula adherens formation in *Caenorhabditis elegans* requires dlg-1, the homologue of the *Drosophila* gene discs large. *Dev. Biol.* 230:29–42. doi:10.1006/dbio.2000.0113

Chisholm, A.D., and J. Hardin. 2005. Epidermal morphogenesis. *WormBook*, editor. The *C. elegans* Research Community, WormBook. doi/10.1895/wormbook.1.35.1. http://www.wormbook.org.

Costa, M., W. Raich, C. Agbunag, B. Leung, J. Hardin, and J.R. Priess. 1998. A putative catenin–cadherin system mediates morphogenesis of the *Caenorhabditis elegans* embryo. *J. Cell Biol.* 141:297–308. doi:10.1083/jcb.141.1.297

Dharmalingam, E., A. Haeckel, R. Pinyol, L. Schwintzer, D. Koch, M.M. Kessels, and B. Qualmann. 2009. F-BAR proteins of the syndapin family shape the plasma membrane and are crucial for neuromorphogenesis. *J. Neurosci.* 29:13315–13327. doi:10.1523/JNEUROSCI.3973-09.2009

Ding, M., W.M. Woo, and A.D. Chisholm. 2004. The cytoskeleton and epidermal morphogenesis in *C. elegans*. *Exp. Cell Res.* 301:84–90. doi:10.1016/j.yexcr.2004.08.017

Dupuy, D., N. Bertin, C.A. Hidalgo, K. Venkatesan, D. Tu, D. Lee, J. Rosenberg, N. Svrzikapa, A. Blanc, A. Carnec, et al. 2007. Genome-scale analysis of in vivo spatiotemporal promoter activity in *Caenorhabditis elegans*. *Nat. Biotechnol.* 25:663–668. doi:10.1038/nbt1305

Endris, V., B. Wogatzky, U. Leimer, D. Bartsch, M. Zatyka, F. Latif, E.R. Maher, G. Tariverdian, S. Kirsch, D. Karch, and G.A. Rappold. 2002. The novel Rho-GTPase activating gene MEGAP/ srGAP3 has a putative role in severe mental retardation. *Proc. Natl. Acad. Sci. USA.* 99:11754–11759. doi:10.1073/pnas.162241099

Frost, A., R. Perera, A. Roux, K. Spasov, O. Destaing, E.H. Egelman, P. De Camilli, and V.M. Unger. 2008. Structural basis of membrane invagination by F-BAR domains. *Cell.* 132:807–817. doi:10.1016/j.cell.2007.12.041

Gallop, J.L., and H.T. McMahon. 2005. BAR domains and membrane curvature: bringing your curves to the BAR. *Biochem. Soc. Symp.* 72:223–231.

Gallop, J.L., C.C. Jao, H.M. Kent, P.J. Butler, P.R. Evans, R. Langen, and H.T. McMahon. 2006. Mechanism of endophilin N-BAR domain-mediated membrane curvature. *EMBO J.* 25:2898–2910. doi:10.1038/sj.emboj.7601174

Guerrier, S., J. Coutinho-Budd, T. Sassa, A. Gresset, N.V. Jordan, K. Chen, W.L. Jin, A. Frost, and F. Polleux. 2009. The F-BAR domain of srGAP2 induces membrane protrusions required for neuronal migration and morphogenesis. *Cell.* 138:990–1004. doi:10.1016/j.cell.2009.06.047

Hekimi, S., P. Boutis, and B. Lakowski. 1995. Viable maternal-effect mutations that affect the development of the nematode *Caenorhabditis elegans*. *Genetics.* 141:1351–1364.

Henne, W.M., H.M. Kent, M.G. Ford, B.G. Hegde, O. Daumke, P.J. Butler, R. Mittal, R. Langen, P.R. Evans, and H.T. McMahon. 2007. Structure and analysis of FCHo2 F-BAR domain: a dimerizing and membrane recruitment module that effects membrane curvature. *Structure.* 15:839–852. doi:10.1016/j.str.2007.05.002

Itoh, T., K.S. Erdmann, A. Roux, B. Habermann, H. Werner, and P. De Camilli. 2005. Dynamin and the actin cytoskeleton cooperatively regulate plasma membrane invagination by BAR and F-BAR proteins. *Dev. Cell.* 9:791–804. doi:10.1016/j.devcel.2005.11.005

Köppen, M., J.S. Simske, P.A. Sims, B.L. Firestein, D.H. Hall, A.D. Radice, C. Rongo, and J.D. Hardin. 2001. Cooperative regulation of AJM-1 controls junctional integrity in *Caenorhabditis elegans* epithelia. *Nat. Cell Biol.* 3:983–991. doi:10.1038/ncb1101-983

Krugmann, S., I. Jordens, K. Gevaert, M. Driessens, J. Vandekerckhove, and A. Hall. 2001. Cdc42 induces filopodia by promoting the formation of an IRSp53:Mena complex. *Curr. Biol.* 11:1645–1655. doi:10.1016/S0960-9822(01)00506-1

Labouesse, M. 2006. Epithelial junctions and attachments. *WormBook*, editor. The *C. elegans* Research Community, WormBook. doi/10.1895/wormbook.1.56.1. http://www.wormbook.org.

Lee, S.H., F. Kerff, D. Chereau, F. Ferron, A. Klug, and R. Dominguez. 2007. Structural basis for the actin-binding function of missing-in-metastasis. *Structure.* 15:145–155. doi:10.1016/j.str.2006.12.005

Li, X., Y. Chen, Y. Liu, J. Gao, F. Gao, M. Bartlam, J.Y. Wu, and Z. Rao. 2006. Structural basis of Robo proline-rich motif recognition by the srGAP1 Src homology 3 domain in the Slit-Robo signaling pathway. *J. Biol. Chem.* 281:28430–28437. doi:10.1074/jbc.M604135200

Lim, K.B., W. Bu, W.I. Goh, E. Koh, S.H. Ong, T. Pawson, T. Sudhaharan, and S. Ahmed. 2008. The Cdc42 effector IRSp53 generates filopodia by coupling membrane protrusion with actin dynamics. *J. Biol. Chem.* 283:20454–20472. doi:10.1074/jbc.M710185200

Lockwood, C., R. Zaidel-Bar, and J. Hardin. 2008. The *C. elegans* zonula occludens ortholog cooperates with the cadherin complex to recruit actin during morphogenesis. *Curr. Biol.* 18:1333–1337. doi:10.1016/j.cub.2008.07.086

Lynch, A.M., and J. Hardin. 2009. The assembly and maintenance of epithelial junctions in *C. elegans*. *Front. Biosci.* 14:1414–1432. doi:10.2741/3316

Masuda, M., S. Takeda, M. Sone, T. Ohki, H. Mori, Y. Kamioka, and N. Mochizuki. 2006. Endophilin BAR domain drives membrane curvature by two newly identified structure-based mechanisms. *EMBO J.* 25:2889–2897. doi:10.1038/sj.emboj.7601176

Nance, J., and J.R. Priess. 2002. Cell polarity and gastrulation in *C. elegans*. *Development.* 129:387–397.

Peter, B.J., H.M. Kent, I.G. Mills, Y. Vallis, P.J. Butler, P.R. Evans, and H.T. McMahon. 2004. BAR domains as sensors of membrane curvature: the amphiphysin BAR structure. *Science.* 303:495–499. doi:10.1126/science.1092586

Pettitt, J., E.A. Cox, I.D. Broadbent, A. Flett, and J. Hardin. 2003. The *Caenorhabditis elegans* p120 catenin homologue, JAC-1, modulates cadherin–catenin function during epidermal morphogenesis. *J. Cell Biol.* 162:15–22. doi:10.1083/jcb.200212136

Piekny, A.J., and P.E. Mains. 2003. Squeezing an egg into a worm: *C. elegans* embryonic morphogenesis. *ScientificWorldJournal.* 3:1370–1381. doi:10.1100/tsw.2003.123

Priess, J.R., and D.I. Hirsh. 1986. *Caenorhabditis elegans* morphogenesis: the role of the cytoskeleton in elongation of the embryo. *Dev. Biol.* 117:156–173. doi:10.1016/0012-1606(86)90358-1

Raich, W.B., C. Agbunag, and J. Hardin. 1999. Rapid epithelial-sheet sealing in the *Caenorhabditis elegans* embryo requires cadherin-dependent filopodial priming. *Curr. Biol.* 9:1139–1146. doi:10.1016/S0960-9822(00)80015-9

Rao, Y., Q. Ma, A. Vahedi-Faridi, A. Sundborger, A. Pechstein, D. Puchkov, L. Luo, O. Shupliakov, W. Saenger, and V. Haucke. 2010. Molecular basis for SH3 domain regulation of F-BAR-mediated membrane deformation. *Proc. Natl. Acad. Sci. USA.* 107:8213–8218. doi:10.1073/pnas.1003478107

Saarikangas, J., H. Zhao, A. Pykäläinen, P. Laurinmäki, P.K. Mattila, P.K. Kinnunen, S.J. Butcher, and P. Lappalainen. 2009. Molecular mechanisms of membrane deformation by I-BAR domain proteins. *Curr. Biol.* 19:95–107. doi:10.1016/j.cub.2008.12.029

Sheffield, M., T. Loveless, J. Hardin, and J. Pettitt. 2007. *C. elegans* Enabled exhibits novel interactions with N-WASP, Abl, and cell-cell junctions. *Curr. Biol.* 17:1791–1796. doi:10.1016/j.cub.2007.09.033

Shimada, A., H. Niwa, K. Tsujita, S. Suetsugu, K. Nitta, K. Hanawa-Suetsugu, R. Akasaka, Y. Nishino, M. Toyama, L. Chen, et al. 2007. Curved EFC/F-BAR-domain dimers are joined end to end into a filament for membrane invagination in endocytosis. *Cell.* 129:761–772. doi:10.1016/j.cell.2007.03.040

Shimada, A., K. Takano, M. Shirouzu, K. Hanawa-Suetsugu, T. Terada, K. Toyooka, T. Umehara, M. Yamamoto, S. Yokoyama, and S. Suetsugu. 2010. Mapping of the basic amino-acid residues responsible for tubulation and cellular protrusion by the EFC/F-BAR domain of pacsin2/Syndapin II. *FEBS Lett.* 584:1111–1118. doi:10.1016/j.febslet.2010.02.058

Soderling, S.H., K.L. Binns, G.A. Wayman, S.M. Davee, S.H. Ong, T. Pawson, and J.D. Scott. 2002. The WRP component of the WAVE-1 complex attenuates Rac-mediated signalling. *Nat. Cell Biol.* 4:970–975. doi:10.1038/ncb886

Timmons, L. 2006. Delivery methods for RNA interference in *C. elegans*. *Methods Mol. Biol.* 351:119–125.

Tsujita, K., S. Suetsugu, N. Sasaki, M. Furutani, T. Oikawa, and T. Takenawa. 2006. Coordination between the actin cytoskeleton and membrane deformation by a novel membrane tubulation domain of PCH proteins is involved in endocytosis. *J. Cell Biol.* 172:269–279. doi:10.1083/jcb.200508091

Vasioukhin, V., C. Bauer, M. Yin, and E. Fuchs. 2000. Directed actin polymerization is the driving force for epithelial cell-cell adhesion. *Cell.* 100:209–219. doi:10.1016/S0092-8674(00)81559-7

Vogt, D.L., C.D. Gray, W.S. Young III, S.A. Orellana, and A.T. Malouf. 2007. ARHGAP4 is a novel RhoGAP that mediates inhibition of cell motility and axon outgrowth. *Mol. Cell. Neurosci.* 36:332–342. doi:10.1016/j.mcn.2007.07.004

Weissenhorn, W. 2005. Crystal structure of the endophilin-A1 BAR domain. *J. Mol. Biol.* 351:653–661. doi:10.1016/j.jmb.2005.06.013

Williams-Masson, E.M., A.N. Malik, and J. Hardin. 1997. An actin-mediated two-step mechanism is required for ventral enclosure of the *C. elegans* hypodermis. *Development.* 124:2889–2901.

Wong, K., X.R. Ren, Y.Z. Huang, Y. Xie, G. Liu, H. Saito, H. Tang, L. Wen, S.M. Brady-Kalnay, L. Mei, et al. 2001. Signal transduction in neuronal migration: roles of GTPase activating proteins and the small GTPase Cdc42 in the Slit-Robo pathway. *Cell.* 107:209–221. doi:10.1016/S0092-8674(01)00530-X

Yang, C., M. Hoelzle, A. Disanza, G. Scita, and T. Svitkina. 2009. Coordination of membrane and actin cytoskeleton dynamics during filopodia protrusion. *PLoS One.* 4:e5678. doi:10.1371/journal.pone.0005678

Yang, Y., M. Marcello, V. Endris, R. Saffrich, R. Fischer, M.F. Trendelenburg, R. Sprengel, and G. Rappold. 2006. MEGAP impedes cell migration via regulating actin and microtubule dynamics and focal complex formation. *Exp. Cell Res.* 312:2379–2393. doi:10.1016/j.yexcr.2006.04.001

Published November 8, 2010

Zaidel-Bar et al., http://www.jcb.org/cgi/content/full/jcb.201005082/DC1

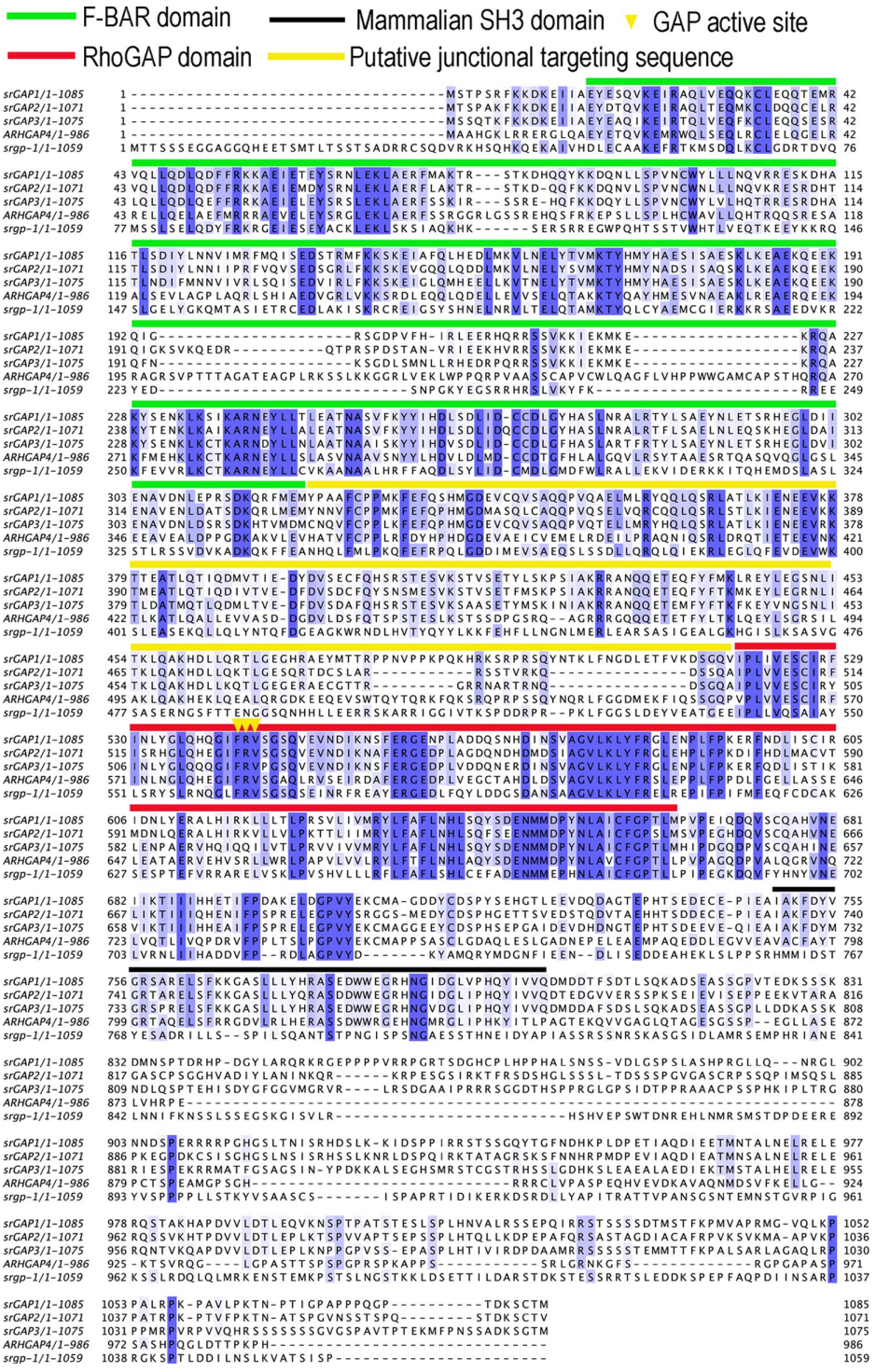

Figure S1. **Multiple alignment of *C. elegans* SRGP-1 with human srGAP family members.** The full protein sequences of *C. elegans* SRGP-1 and human srGAP1, srGAP2, srGAP3, and ARHGAP4 were aligned using ClustalW. A high degree of conservation is found along the F-BAR and GAP domains, as well as regions between them (putative junctional targeting sequence) and immediately after the GAP domain. However, the SH3 domain is not conserved in SRGP-1. Dark blue highlight marks residues that are conserved between all five sequences, and light blue highlight marks residues that are conserved in four out of five of the sequences.

Published November 8, 2010

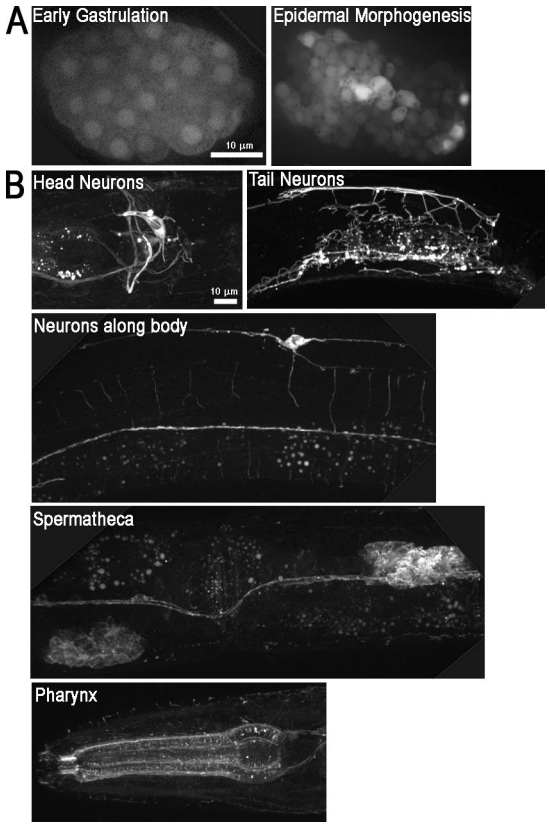

Figure S2. **Expression pattern of the *srgp-1* promoter.** An extrachromosomal array, *sEx10607*, was used to visualize the expression of cytoplasmic GFP driven by the *srgp-1* promoter. (A) In the embryo, *srgp-1* is first expressed in all cells, and later, expression is restricted to neuroblasts, epidermal, and pharyngeal cells. (B) In adults, expression is seen in the nervous system as well as in the pharynx and spermatheca.

Published November 8, 2010

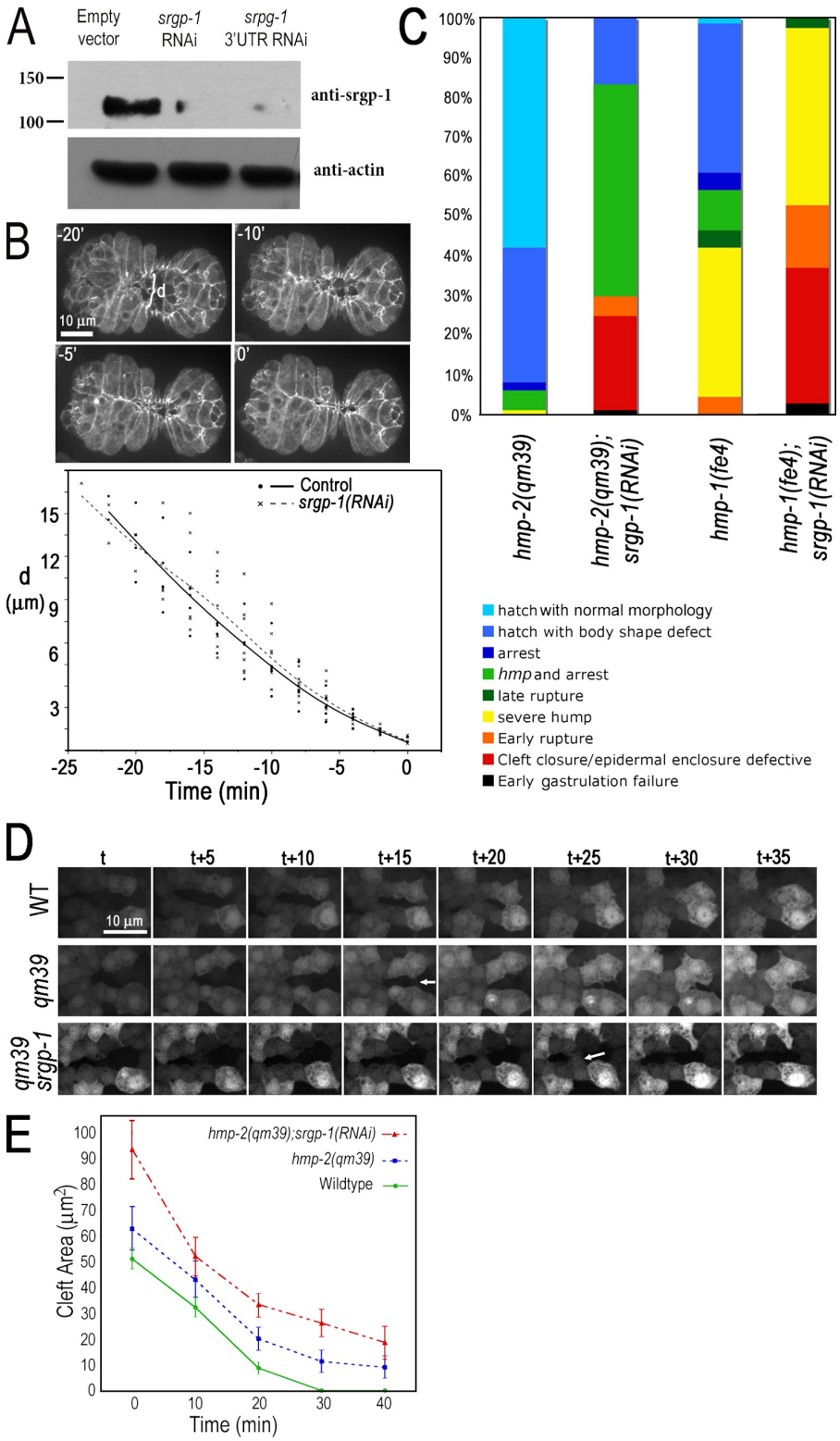

Figure S3. **Knockdown of *srgp-1* enhances lethality and leads to more severe defects in hmp-1/α-catenin and hmp-2/β-catenin hypomorphs.** (A) Western blot showing the knockdown of SRGP-1 by feeding *srgp-1(RNAi)*. Numbers on the left are in given kilodaltons. (B) Quantification of ventral closure rate in control and *srgp-1(RNAi)* embryos expressing HMP-1::GFP. d is the distance between two opposing epidermal cells that was measured and used to quantify the rate of ventral enclosure as shown in the graph. (C) Nomarski videos of single and double mutants were analyzed to determine the earliest failure and lethal phenotype (defined in the legend). The bar chart represents pooled data from three or more videos for each genotype ($n > 60$). (D) Comparison of cleft closure in wild-type, *hmp-2(qm39)*, and *hmp-2(qm39);srgp-1(RNAi)* embryos shows rapid and irreversible sealing of the cleft in wild type compared with adhesion and deadhesion events in the mutants (arrows), which lead to slower closure in the single mutant and widening of the cleft in the double mutant. WT, wild type. (E) Quantification of cleft area versus time. Lines depict the mean from more than six individual embryos, and error bars denote SEM.

Published November 8, 2010

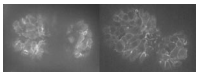

Video 1. **Ventral enclosure in wild-type and *srgp-1(RNAi)* embryos.** HMP-1::GFP dynamics show extensive membrane ruffling (arrows) and rapid junction formation in wild type versus less membrane ruffling and slower junction formation in the *srgp-1(RNAi)* embryo. Single focal plane. Frames are shown at 1 min apart. Play rate is nine frames per second.

Video 2. **Morphogenetic failure in *hmp-1(fe4)*/α-catenin;*srgp-1* double mutant embryos.** One Z section from a Nomarski time-lapse video following the development of *hmp-1(fe4);srgp-1(RNAi)* embryos from the four-cell stage. All embryos fail in gastrulation cleft closure and subsequently rupture from the cleft. Play rate is nine frames per second.

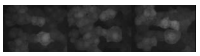

Video 3. **Gastrulation cleft closure in wild type, catenin single mutant, and double *hmp-2(qm39)*/β-catenin;*srgp-1(RNAi)* mutants.** Single Z section, 1-min interval time-lapse videos of cleft closure in wild-type (left), *hmp-2(qm39)* (middle), and *hmp-2(qm39);srgp-1(RNAi)* embryos. Note the faster closure in wild-type embryos and the separation of cells that have already made contact in the mutant embryos. Play rate is nine frames per second.

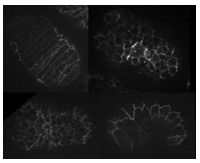

Video 4. **Dynamics of SRGP-1::GFP at various developmental stages.** Time-lapse videos of SRGP-1::GFP were acquired at 1-min intervals. Each frame is a projection of eight Z sections spaced 0.2 μm apart. On the top left is a dorsal view of epidermal cells after intercalation; on the top right is a ventral view during late gastrulation. On the bottom left is a view of ventral epidermal enclosure, and on the bottom right is epidermal elongation. Play rate is nine frames per second.